Carbon Letters (2020) 30:485–491
https://doi.org/10.1007/s42823-019-00118-9

Online ISSN 2233-4998
Print ISSN 1976-4251

ORIGINAL ARTICLE

Production of NiO/N-doped carbon hybrid and its electrocatalytic performance for oxygen evolution reactions

Sujin Seok[1] · Dawoon Jang[1] · Haeju Kim[1] · Sungjin Park[1]

Received: 29 August 2019 / Revised: 26 November 2019 / Accepted: 17 December 2019 / Published online: 3 January 2020

Abstract

Oxygen evolution reaction (OER) is an essential step at an anode in electrochemical water-splitting process and requires efficient electrocatalysts to reduce overpotentials. Although precious metal-based materials, such as RuO_2, IrO_2 and their hybrids with other components, performed excellently as OER electrocatalysts, their high cost has limited practical applications. Consequently, earth-abundant metal components including Fe, Co, and Ni have been investigated as alternatives. In this work, the hybridization of Ni-containing species with conductive carbon-based materials was used to prevent aggregation of active species and improve electrochemical catalytic performance. A new hybrid material composed of NiO nanoparticles and N-doped carbon materials was prepared. The NiO particles with a narrow size distribution were well dispersed on the surface of carbon-based materials. The hybrid showed improved electrocatalytic performance for OER than single components of NiO and N-doped carbon materials.

Keywords Oxygen evolution reactions · Nickel oxides · N-doped carbon materials

Water splitting is an important process for renewable and environment-friendly energy-storage systems [1]. The oxygen evolution reaction (OER) is an essential step at an anode during electrochemical water-splitting process [2] and requires efficient electrocatalysts to reduce overpotentials [2, 3].

Although precious metal-based materials, such as RuO_2, IrO_2 and their hybrids with other components, showed excellent properties as OER electrocatalysts, the high cost has limited their practical applications [4]. Consequently, earth-abundant metal components including Fe, Co, and Ni have been investigated as alternative electrocatalysts [5]. The previous study suggested that Ni-based materials are good candidates due to the good interaction ability of Ni-containing active species with a reaction intermediate, OH_{ad} [6]. Various materials, such as NiP_2, Ni chalcogenides, nickel hydroxide, and nickel oxides, exhibit promising properties such as low overpotentials for OER in alkaline electrolytes. However, their low conductivity and slow kinetics for OER limited to reach the maximum catalytic performance [7–9].

Carbon-based nanomaterials, such as chemically modified graphenes, carbon nanotubes, carbon nitrides, and activated carbons have been widely used as supports for various electrocatalysts [10]. Due to their high surface areas, fast electron transfer, and tunable chemical properties, they often enhance electrocatalytic performance when metal-containing active species are uniformly dispersed at the surface of the carbon-based materials [11]. Specially, the achievement of uniform dispersion is one of the critical points to enhance catalytic performance. Additionally, it is frequently reported that N-doping into the carbon network is advantageous to improve the electrocatalytic properties [10, 12]. Recently, theoretical calculations also suggested that Ni species dispersed on the carbon-based network can have low activation energy for OER [13, 14]. In this work, the hybridization of Ni-containing species with conductive carbon-based materials was used to prevent aggregation of active species and improve electrochemical catalytic performance. We studied the preparation of a novel hybrid consisting of NiO particles dispersed on N-doped sp^2 carbon network and their electrocatalytic performance for the OER.

To achieve good dispersion of Ni species on carbon-based supports, $Ni(II)Cl_2(H_2O)_6$ (200 mg, 99.999%,

✉ Sungjin Park
sungjinpark@inha.ac.kr

[1] Department of Chemistry and Chemical Engineering, Inha University, 100 Inha-ro, Michuhol-gu, Incheon 22212, Republic of Korea

Sigma-Aldrich) and urea (2 g, 99%, Sigma-Aldrich) were dissolved in a 100 mL beaker filled with 10 mL of ethanol (Fig. 1). The mixture was heated in an oil bath set at 80 °C then was stirred for 12 h to remove ethanol. The resulting wet mixture was dried under vacuum at room temperature until the dried powder was obtained. The powder was placed in a quartz crucible and then covered with a cap. The crucible was then placed in the center of a quartz tube. After putting the tube into a furnace (TFP-80-3, Dongseo Science Co., Ltd., Korea) linked with H_2O bubbling trap, the temperature was increased to 520 °C with a heating rate of 10 °C/min and held at 520 °C for 2 h under H_2O bubbling. After cooling to room temperature, the product (51 mg, NiO/NC) was obtained as a dark green powder. As a reference sample, urea was heated without the presence of $Ni(II)Cl_2(H_2O)_6$, affording pale yellow powder (CN).

The high-resolution scanning electron microscopy (HR-SEM) images of Pt-coated samples were obtained using a field-emission SEM system (S-4300SE, Hitachi) at an accelerating voltage of 15 kV. Transmission electron microscopy (TEM) analyses were conducted with a CM200 instrument (Philips) at 200 kV with samples on a holey carbon supported on a 200 mesh copper grid (HC200CU, EMS, USA). Energy-dispersive X-ray spectroscopy (EDX) with elemental mapping was conducted with JEM2100F/JEOL instrument (JEOL, Japan) at 200 kV with samples on a holey carbon supported on a 200 mesh copper grid (HC200CU, EMS, USA). The powder X-ray diffraction (XRD) patterns were taken on Multi-Purpose X-ray Diffractometer (X'Pert Powder Diffractometer, PANalytical). X-ray photoelectron spectroscopy (XPS) spectra of samples were obtained using high-performance XPS (HP-XPS, Theta probe, Thermo Electron Cooperation) and binding energies were determined versus the C 1 *s* peak at 284.6 eV, which is assigned to sp^2 carbons.

Electrochemical experiments were performed using a VSP analyzer (BioLogic, France) at room temperature. An electrochemical cell was constructed using the three-compartment electrochemical cell, consisting of a sample-modified glassy carbon rotating disk electrode (GC RDE) working electrode, a Pt wire counter electrode, and Hg/HgO (1 M NaOH) as a reference electrode. Sample-loading solutions (2.5 mg of sample and 20 µL Nafion (5%, Aldrich) were dispersed in 980 µL DI water/ethanol (1:1 (v/v)) mixed by sonication at least 200 min. Next, 10 µL of the loading solution was dropped on the cleaned GC RDE and dried for 1 h. Before the test, the 1 M KOH electrolyte solution was purged with N_2 for 1 h. For OER measurements, the linear sweep voltammetry (LSV) was performed from 1.2 to 1.8 V (vs reversible hydrogen electrode (RHE)) at a scan rate of 5 mV/s with 1600 rpm. Electrochemical impedance spectroscopy (EIS) was obtained at 1.7 V (vs RHE). Before all the analysis, cyclic voltammetry (CV) were performed 50 cycles from 1.2 to 1.8 V. The chronoamperometry (CA) tests were done at 1.7 V for 5000 s. Cyclic tests were conducted with CV scans between 1.23 and 1.73 V for 1000 cycles. For convenient comparison, all potentials were referenced relative to a RHE according to the following equation:

$$E_{RHE} = E_{Hg/HgO} + 0.14 + 0.059\,pH.$$

Agglomerated carbon-based particles were found in the SEM image of the NiO/NC powder (Fig. 2a). The TEM image showed well-dispersed particles with several of nm in length on the amorphous carbon-based materials (Fig. 2b). No aggregated particles were observed in TEM image, which is beneficial to achieve high catalytic performance. The averaged size of the particles, which was determined with 45 particles in TEM images, was 2.5 ± 0.13 nm with narrow size distribution (Fig. 2c).

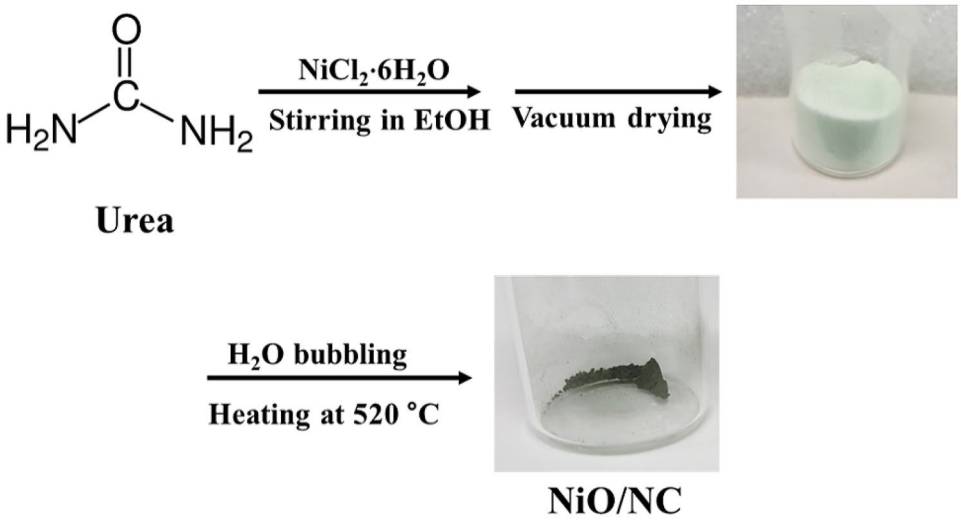

Fig. 1 A scheme for the production of NiO/NC material

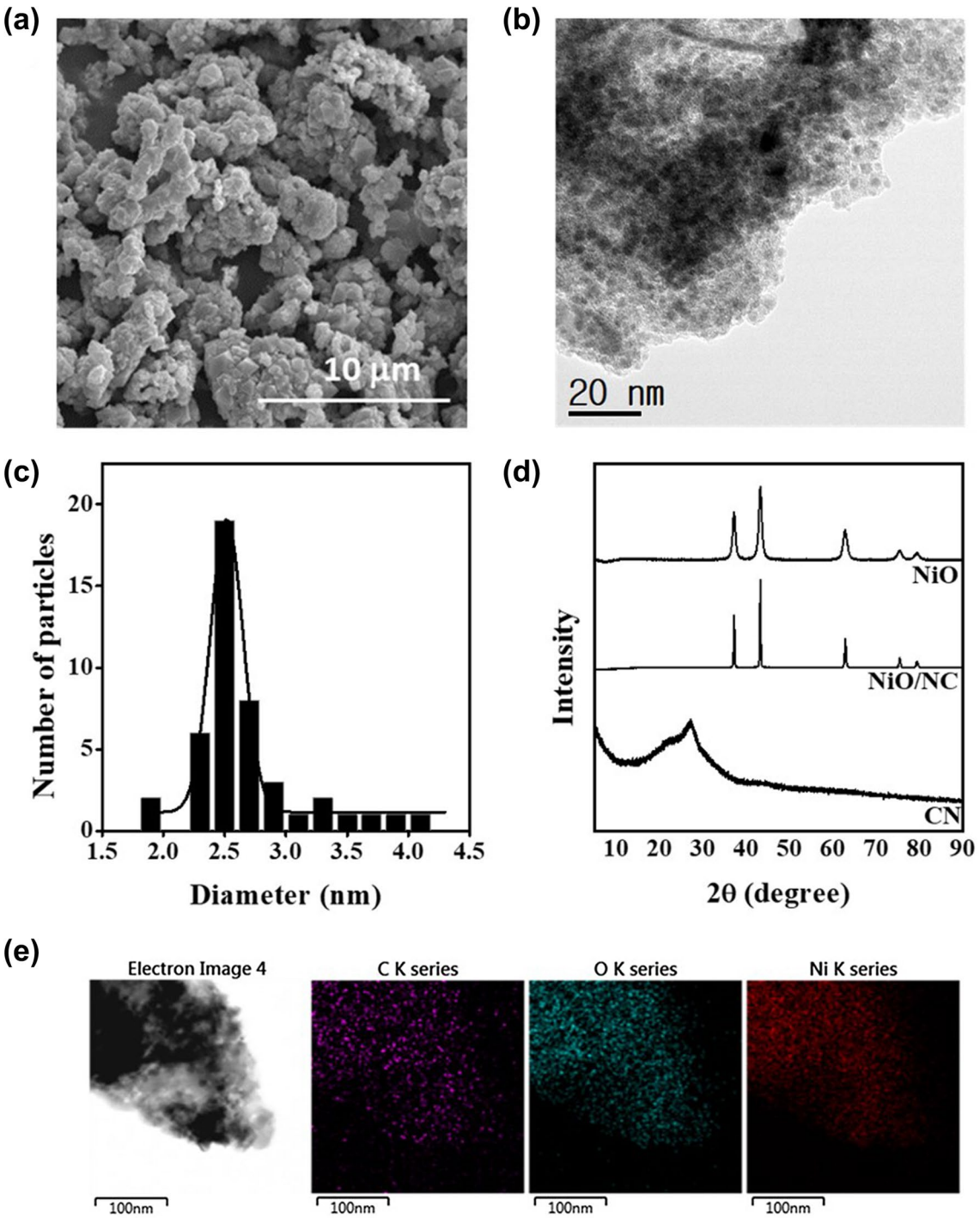

Fig. 2 **a** An SEM image and **b** a TEM image of NiO/NC, **c** a size distribution of NiO particles measured on the TEM image, **d** XRD patterns of NiO, NiO/NC, and CN, and **e** TEM and elemental mapping images of NiO/NC

We further analyzed the structure of NiO/NC material with chemical characterizations. It is well known that the heat treatment of urea produced three-dimensional carbon nitride (C_3N_4) by polycondensation [15, 16]. The presence of the C_3N_4 network can be determined by the chemical analysis such as XRD and XPS. While the XRD pattern of CN displayed a broad peak typical for the urea-driven C_3N_4 materials (Fig. 2d), that of NiO/NC did sharp peaks at 37.2°, 43.3°, 62.8°, 75.4°, and 79.4°, corresponding to (111), (200), (220), (311), and (222) planes of crystalline NiO particles, respectively, without peaks for C_3N_4 [17, 18]. The elemental mapping images (Fig. 2e) show Ni and O are well dispersed

on the N-doped carbons. Therefore, we suggested that N-doped carbon supports prevented the aggregation of NiO particles, leading to the improved electrocatalytic properties.

Elemental amounts of the samples were determined with XPS measurements. The CN was composed of mostly C and N atoms with ~ 48 and ~ 47 at.%, respectively, in Table 1. On the other hands, NiO/NC contained only 1 at.% of N atoms and a reduced amount of C atoms with ~ 29 at.%. It suggests that the main frame of NiO/NC is carbon-based materials with small amounts of N atoms doped in carbon network. The elemental amounts of Ni and O atoms of NiO/NC were ~ 27 and ~ 44 at.%, respectively, supporting the formation of NiO structure. Because NiO contains 1:1 atomic ratio of Ni and O, some O atoms attached to the carbon network. The deconvoluted XPS Ni 2*p* spectrum of NiO/NC showed peaks at ~ 854 eV ($2p_{3/2}$) and ~ 872 eV ($2p_{1/2}$) and a satellite for each (Fig. 3a). The difference between the binding energies is 18.5 eV, indicating the presence of NiO particles [19, 20]. The deconvoluted C *1s* spectrum of NiO/NC shows a main peak at 284.6 eV, which means the presence of sp^2 carbon network as a main framework. Additionally, peaks at 285.6, 286.3, 288.2, and 289.0 eV, which are assignable to C–OH, C–O, C=O, and O–C=O, were found (Fig. 3b) [21]. The deconvoluted N 1*s* spectrum showed peaks at 398.6, 399.8, 401.0, and 401.9 eV, which are assignable to pyridinic, pyrrolic, graphitic, and oxidized N (Fig. 3c) [22]. The deconvoluted O 1*s* spectrum found peaks at 529.2, 531.2, and 534.0 eV, corresponding to Ni–O, C=O/Ni–O, and C–O (Fig. 3d). Additionally, the peak at 530.2 eV could be attributed to the formation of Ni–O–C moieties, suggesting the presence of Ni species bound with carbon-based network [19, 21, 23].

The FT-IR spectrum of NiO/NC found the presence of NiO particles with a peak at 442 cm^{-1}, corresponding to Ni–O moieties (Fig. 4a,b). Other peaks at 675, 808, 1053, 1261, 1323, 1632, and 3423 cm^{-1} correspond to Ni–O, N–H,

Table 1 Atomic percents of CN and NiO/NC

At.%	CN	NiO/NC
C	48.4	28.8
N	47.3	1.1
Ni		26.6
O	4.3	43.6

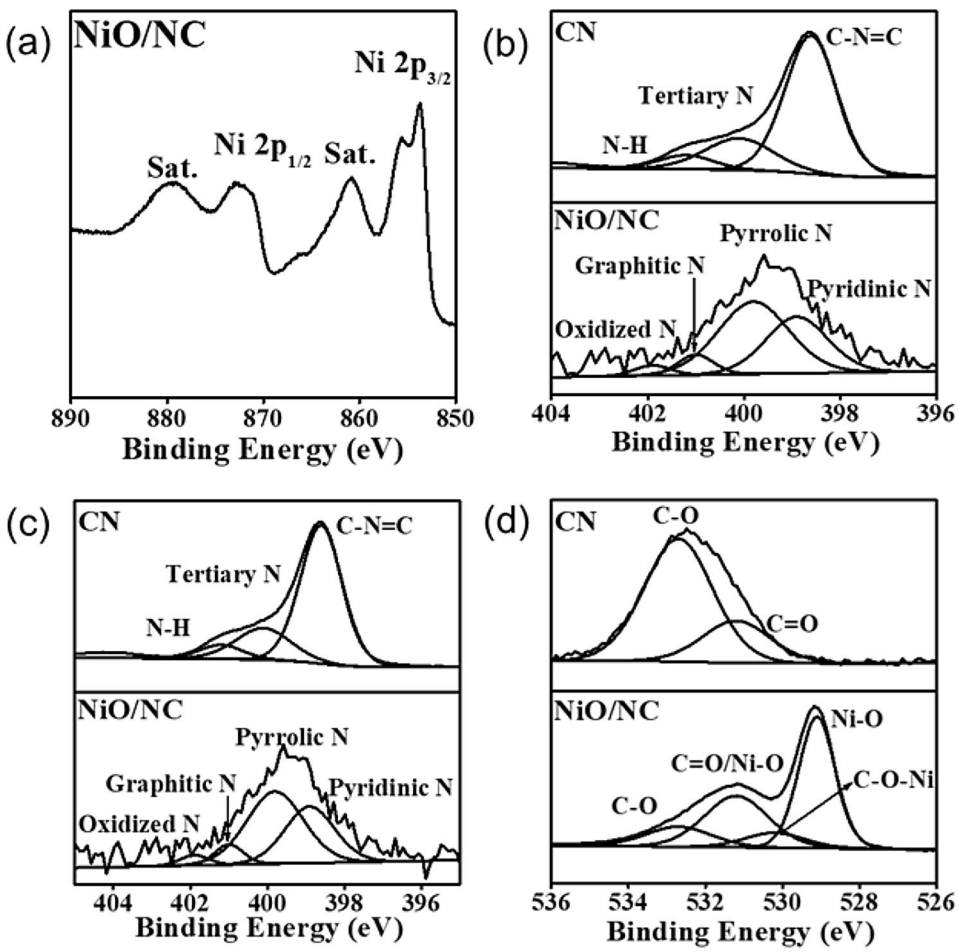

Fig. 3 **a** An XPS Ni 2*p* spectrum of NiO/NC and deconvoluted XPS spectra of CN and NiO/NC for **b** C 1*s*, **c** N 1*s*, and **d** O 1*s*

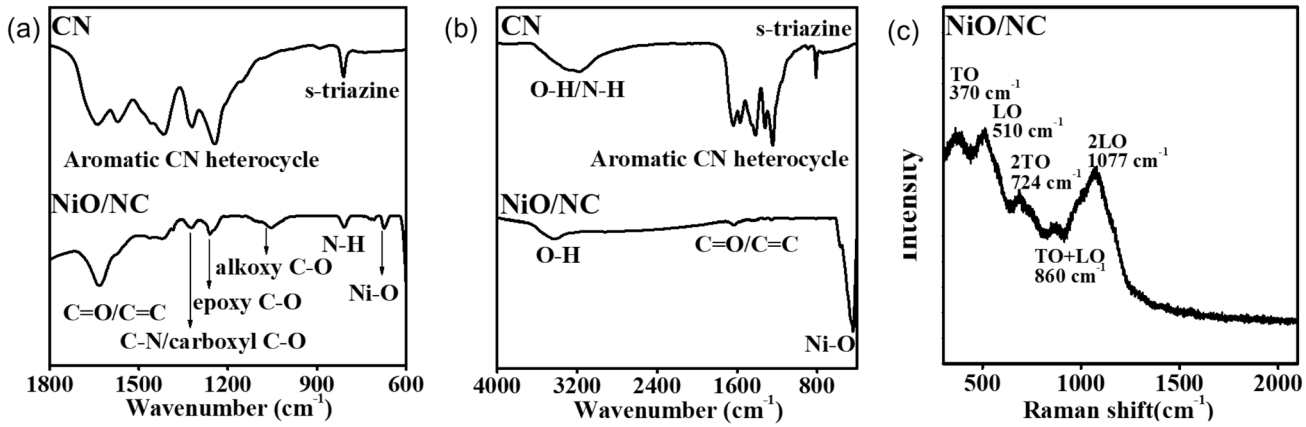

Fig. 4 **a** FT-IR spectrum of CN and NiO/NC at the selected region, **b** at the wide region, and **c** Raman spectrum of NiO/NC

Table 2 Electrocatalytic OER performance of the samples

	CN	A-rG-O	NiO/NC	NiO
Onset potential(V)	1.62	1.61	1.54	1.55
Potential (V)@ 10 mA/cm^2			1.65	1.69
Overpotential (mV) @ 10 mA/cm^2			420	460

C–O in alkoxy, C–O in epoxy, C–N/C–O in carboxyl, C=O/C=C, and O–H moieties, respectively (Fig. 4a, b) [13, 23]. As shown in Fig. 4c, the Raman spectrum of NiO/NC was almost identical to that of NiO [18, 23]. All characterizations confirmed that small-sized NiO particles were generated on the N-doped carbon materials.

We tested electrocatalytic performance of the hybrid for OER in 1 M KOH solution. Figure 5a shows LSV curves of NiO/NC, CN, A-rG-O, and NiO at a scan rate of 5 mV/s using a RDE. The overpotential is a common indicator for OER catalytic activity and was calculated by subtracting 1.23 V (a half-cell potential for water-splitting reaction) from the measured potential at 10 mA cm^{-2} of current density [24]. The onset potentials were determined at the voltage where the currents start to flow. The NiO/NC hybrid exhibited electrocatalytic activity for OER with onset and overpotentials of 1.54 V and 420 mV, respectively, which were lower than those of CN, A-rG-O, and NiO (Table 2). The Tafel slope, which describes the influence of potential, or overpotential on steady-state current density, is an important factor for the evaluation of OER kinetics [25]. The Tafel slopes were calculated from the LSV curves at a scan rate of 1600 rpm. The Tafel slope (61 mV/dec) of NiO/NC was lower than those of CN (229 mV/dec), A-rG-O (178 mV/dec), and NiO (78 mV/dec) (Fig. 5b). It is indicative of the faster OER kinetics of the former than the latter. From the Nyquist plots obtained through EIS measurements, the R_1 is solution resistance containing electrolytes and R_2 is the

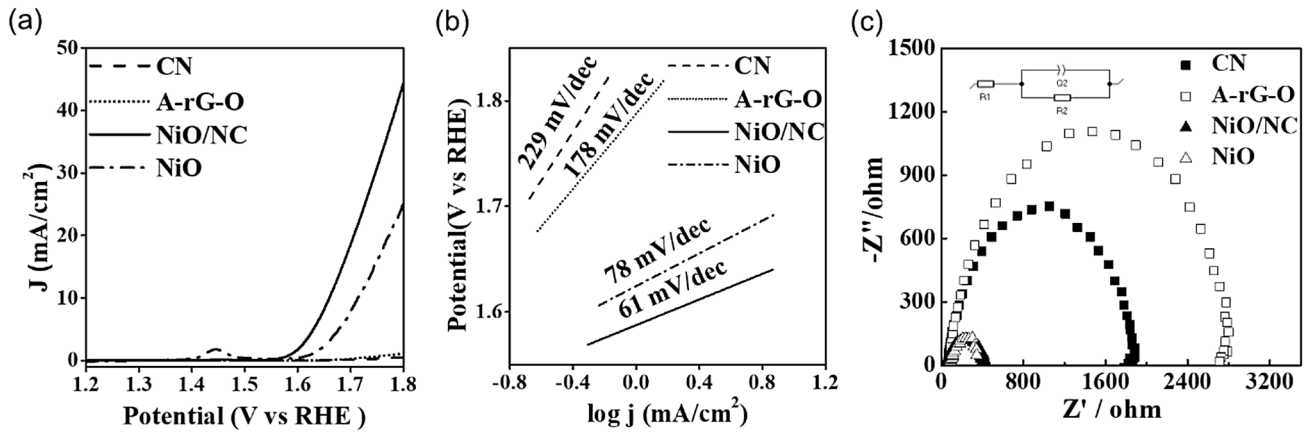

Fig. 5 Electrocatalytic performance of catalyst for OER. **a** LSV curves of CN, A-rG-O, NiO/NC, and NiO, **b** Tafel plots of CN, A-rG-O, NiO/NC, and NiO and **c** EIS measurements at an applied potential of 1.7 V vs. RHE

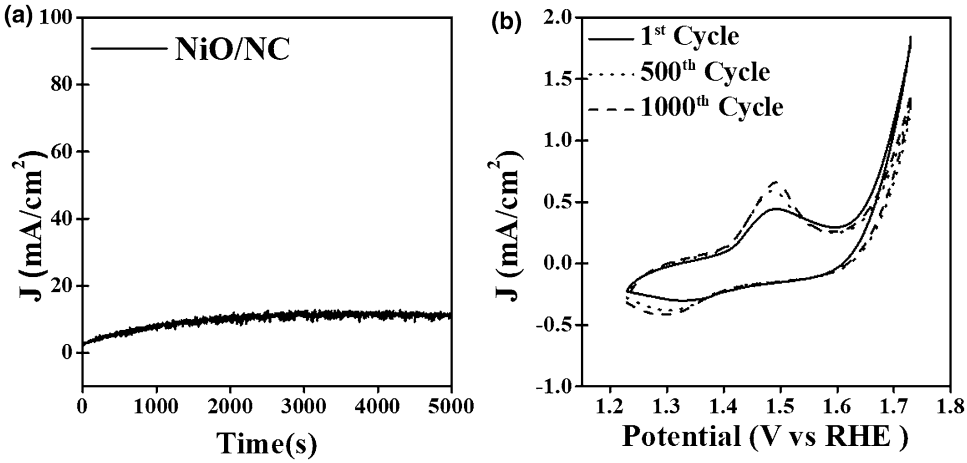

Fig. 6 **a** CA test for NiO/NC at an applied potential of 1.7 V vs. RHE **b** CV curves at 1st, 500th, and 1000th cycles for NiO/NC

charge transfer resistances across the electrode–electrolyte interfaces (R_{ct}), which were calculated using a simple Randles circuit (Fig. 5c). The semicircular diameter size indicated the R_{ct} value [26]. The R_{ct} value (360 Ω) of NiO/NC was much lower than CN (1800 Ω) and A-rG-O (2740 Ω), suggesting the lower interfacial resistance of NiO/NC than carbon-based materials. All these electrochemical experiments support that the hybridization between NiO particles and N-doped carbon-based supports are effective to improve the electrocatalytic activity for OER.

Because the durability is one of the important factors of electrocatalysts, it was monitored with CA and CV cyclic tests. In CA test, NiO/NC showed a stable current profile up to 5000 s (Fig. 6a) and the 1000th CV curve of NiO/NC was almost identical to the others (Fig. 6b). These data support good stability of NiO/NC during electrochemical cycles.

In summary, a new hybrid material (NiO/NC) composed of NiO nanoparticles and N-doped carbon was prepared. The NiO particles with a narrow size distribution were well dispersed on the surface of carbon-based materials. Its morphological and chemical structures were analyzed by XPS, XRD, FT-IR, SEM, and TEM measurements. The NiO/NC showed improved electrocatalytic performance for OER than NiO. These results suggest that Ni-containing carbon hybrid systems could be useful to develop efficient electrocatalysts for OER.

Acknowledgements This work was supported by Inha University. We thank the Busan Center at the Korea Basic Science Institute (KBSI) for the XPS analysis.

References

1. Jamesh MI, Sun X (2018) Recent progress on earth abundant electrocatalysts for oxygen evolution reaction (OER) in alkaline medium to achieve efficient water splitting–a review. J Power Sour 400:31. https://doi.org/10.1016/j.jpowsour.2018.07.125
2. Tahir M, Pan L, Idrees F, Zhang X, Wang L, Zou JJ, Wang ZL (2017) Electrocatalytic oxygen evolution reaction for energy conversion and storage: a comprehensive review. Nano Energy 37:136. https://doi.org/10.1016/j.nanoen.2017.05.022
3. Suen NT, Hung SF, Quan Q, Zhang N, Xu YJ, Chen HM (2017) Electrocatalysis for the oxygen evolution reaction: recent development and future perspectives. Chem Soc Rev 46:337. https://doi.org/10.1039/c6cs00328a
4. Lee Y, Suntivich J, May KJ, Perry EE, Shao-Horn Y (2012) Synthesis and activities of rutile IrO_2 and RuO_2 nanoparticles for oxygen evolution in acid and alkaline solutions. J Phys Chem Lett 3:399. https://doi.org/10.1021/jz2016507
5. Louie MW, Bell AT (2013) An investigation of thin-film Ni–Fe oxide catalysts for the electrochemical evolution of oxygen. J Am Chem Soc 135:12329. https://doi.org/10.1021/ja405351s
6. Subbaraman R, Tripkovic D, Chang KC, Strmcnik D, Paulikas AP, Hirunsit P, Chan M, Greeley J, Stamenkovic V, Markovic NM (2012) Trends in activity for the water electrolyser reactions on 3d M (Ni Co, Fe, Mn) hydr(oxy)oxide catalysts. Nat Mater 11:550. https://doi.org/10.1038/NMAT3313
7. Gao X, Zhang H, Li Q, Yu X, Hong Z, Zhang X, Liang C, Lin Z (2016) Hierarchical NiCo2O4 hollow microcuboids as bifunctional electrocatalysts for overall water-splitting. Angew Chem Int Ed 55:6290. https://doi.org/10.1002/anie.201600525
8. Kale VS, Sim U, Yang J, Jin K, Chae SI, Chang WJ, Sinha AK, Ha H, Hwang CC, An J, Hong HK, Lee Z, Nam KT, Hyeon T (2017) Sulfur-modified graphitic carbon nitride nanostructures as an efficient electrocatalyst for water oxidation. Small 13:1603893. https://doi.org/10.1002/smll.201603893
9. McCrory CC, Jung S, Ferrer IM, Chatman SM, Peters JC, Jaramillo TF (2015) Benchmarking hydrogen evolving reaction and oxygen evolving reaction electrocatalysts for solar water splitting devices. J Am Chem Soc 137:4347. https://doi.org/10.1021/ja510442p
10. Byambasuren U, Jeon Y, Altansukh D, Ji Y, Shul YG (2016) One-step synthesis of dual-transition metal substitution on ionic liquid based N-doped mesoporous carbon for oxygen reduction reaction. Carbon Lett 17:53. https://doi.org/10.5714/cl.2016.17.1.053
11. Ohn S, Kim SY, Mun SK, Oh J, Sa YJ, Park S, Joo SH, Kwon SJ, Park S (2017) Molecularly dispersed nickel-containing species on the carbon nitride network as electrocatalysts for the oxygen evolution reaction. Carbon 124:180. https://doi.org/10.1016/j.carbon.2017.08.039

12. Jiang H, Gu J, Zheng X, Liu M, Qiu X, Wang L, Li W, Chen Z, Ji X, Li J (2019) Defect-rich and ultrathin N doped carbon nanosheets as advanced trifunctional metal-free electrocatalysts for the ORR. OER and HER. Energy Environ Sci 12:322. https://doi.org/10.1039/c8ee03276a
13. Zheng Y, Jiao Y, Zhu Y, Cai Q, Vasileff A, Li LH, Han Y, Chen Y, Qiao SZ (2017) Molecule-level g-C_3N_4 coordinated transition metals as a new class of electrocatalysts for oxygen electrode reactions. J Am Chem Soc 139:3336. https://doi.org/10.1021/jacs.6b13100
14. Fei H, Dong J, Feng Y, Allen CS, Wan C, Volosskiy B, Li M, Zhao Z, Wang Y, Sun H, An P, Chen W, Guo Z, Lee C, Chen D, Shakir I, Liu M, Hu T, Li Y, Kirkland AI, Duan X, Huang Y (2018) General synthesis and definitive structural identification of MN_4C_4 single-atom catalysts with tunable electrocatalytic activities. Nat Catal 1:63. https://doi.org/10.1038/s41929-017-0008-y
15. Chen L, Song J (2017) Tailored graphitic carbon nitride nanostructures: synthesis, modification, and sensing applications. Adv Funct Mater 27:1702695. https://doi.org/10.1002/adfm.201702695
16. Zhu J, Xiao P, Li H, Carabineiro SAC (2014) Graphitic carbon nitride: synthesis, properties, and applications in catalysis. ACS Appl Mater Interfaces 6:16449. https://doi.org/10.1021/am502925j
17. Su Q, Sun J, Wang J, Yang Z, Cheng W, Zhang S (2014) Urea-derived graphitic carbon nitride as an efficient heterogeneous catalyst for CO_2 conversion into cyclic carbonates. Catal Sci Technol 4:1556. https://doi.org/10.1039/c3cy00921a
18. Zhou M, Chai H, Jia D, Zhou W (2014) The glucose-assisted synthesis of a graphene nanosheet–NiO composite for high-performance supercapacitors. New J Chem 38:2320. https://doi.org/10.1039/c3nj01351k
19. Payne BP, Biesinger MC, McIntyre NS (2009) The study of polycrystalline nickel metal oxidation by water vapour. J Electron Spectros Relat Phenomena 175:55. https://doi.org/10.1016/j.elspec.2009.07.006
20. Zhang S, Li J, Wen T, Xu J, Wang X (2013) Magnetic Fe_3O_4@NiO hierarchical structures: preparation and their excellent As(V) and Cr(VI) removal capabilities. Rsc Adv 3:2754. https://doi.org/10.1039/c2ra22495j
21. Liu W, Lu C, Wang X, Liang K, Tay BK (2015) In situ fabrication of three-dimensional, ultrathin graphite/carbon nanotube/NiO composite as binder-free electrode for high-performance energy storage. J Mater Chem A 3:624. https://doi.org/10.1039/c4ta04023f
22. Yan C, Li H, Ye Y, Wu H, Cai F, Si R, Xiao J, Miao S, Xie S, Yang F, Li Y, Wang G, Bao X (2018) Coordinatively unsaturated nickel–nitrogen sites towards selective and high-rate CO_2 electroreduction. Energy Environ Sci 11:1204. https://doi.org/10.1039/c8ee00133b
23. Zhou G, Wang DW, Yin LC, Li N, Li F, Cheng HM (2012) Oxygen bridges between NiO nanosheets and graphene for improvement of lithium storage. ACS Nano 6:3214. https://doi.org/10.1021/nn300098m
24. Huang ZF, Wang J, Peng Y, Jung CY, Fisher A, Wang X (2017) Design of efficient bifunctional oxygen reduction/evolution electrocatalyst: recent advances and perspectives. Adv Energy Mater 7:1700544. https://doi.org/10.1002/aenm.201700544
25. Long X, Li J, Xiao S, Yan K, Wang Z, Chen H, Yang S (2014) A strongly coupled graphene and FeNi double hydroxide hybrid as an excellent electrocatalyst for the oxygen evolution reaction. Angew Chem 126:7714. https://doi.org/10.1002/ange.201402822
26. Kumar V, Appa Rao BV (2017) Chemically modified biopolymer as an eco-friendly corrosion inhibitor for mild steel in a neutral chloride environment. New J Chem 41:6278. https://doi.org/10.1039/c7nj00553a